Procedure for LEED *I-V* structural analysis of metal oxide surfaces: $Ca_{1.5}Sr_{0.5}RuO_4(001)$

V. B. Nascimento,[1,2,*] R. G. Moore,[1,2] J. Rundgren,[3] Jiandi Zhang,[2,4] Lei Cai,[4] R. Jin,[2]
D. G. Mandrus,[1,2] and E. W. Plummer[1,2,5]

[1]*Department of Physics and Astronomy, The University of Tennessee, Knoxville, Tennessee 37996-1200, USA*
[2]*Materials Science and Technology Division, Oak Ridge National Laboratory, Oak Ridge, Tennessee 37831, USA*
[3]*Department of Theoretical Physics, Alba Nova Research Center, Royal Institute of Technology (KTH), SE-106 91 Stockholm, Sweden*
[4]*Department of Physics, Florida International University, Miami, Florida 33199, USA*
[5]*Center for Nanophase Materials Sciences, Oak Ridge National Laboratory, Oak Ridge, Tennessee 37831, USA*

(Received 17 October 2006; published 11 January 2007)

Transition metal oxides (TMOs) are famous for the intimate coupling between the lattice, electrons, and spin, creating exotic functionality. Creating a surface, breaking the symmetry, should result in lattice distortions that due to the close coupling could create different "surface phases." Historically it has been very difficult to use low energy electron diffraction *I-V* to quantitatively determine the surface structure of TMOs. A signature of this problem is the large values commonly reported in the literature of the Pendry reliability factor (R_P), which is used to quantify the agreement between experimental data and calculated diffraction. In this paper we describe a consistent procedure for determining the phase shifts using an optimized muffin-tin potential approach combined with an energy-dependent real and imaginary inner potential. This procedure is used to determine the surface structure of the layered TMO $Ca_{1.5}Sr_{0.5}RuO_4$. An acceptable Pendry reliability factor is achieved (R_P=0.28).

DOI: 10.1103/PhysRevB.75.035408 PACS number(s): 68.35.Bs, 61.14.Hg, 74.70.Pq, 61.14.Dc

I. INTRODUCTION

Transition metal oxides (TMOs) exhibit an exotic array of phases due to the close coupling between the lattice, the charge, and the spin. In many cases this exotic behavior is enhanced by the two-dimensional character of the TMO, and recent experimental and theoretical results indicate that artificially fabricated layered configurations of two or more TMOs can display a functionality dictated by the interface.[1] An obvious place to explore this new physics created by reduced dimensionality or broken symmetry is at the surface of a TMO. In this paper we address the use of low energy electron diffraction (LEED) *I-V* to quantitatively determine the surface structures in TMOs.

The layered TMO, $Ca_{1.5}Sr_{0.5}RuO_4$,[2] was chosen to test our LEED *I-V* procedure. This doped ruthenate presents a very complex structure with five distinct elements (Ca, Sr, Ru, and O in two different structural sites) and a total of 56 atoms in the bulk unit cell. The phase diagram of the $Ca_{2-x}Sr_xRuO_4$ is very rich with what is believed to be a quantum critical point existing at x=0.5.[2] To illustrate the difference between LEED *I-V* data from a TMO and a simple metal surface, Fig. 1(a) is a comparison of data from Cu(100) and $Ca_{1.5}Sr_{0.5}RuO_4(001)$. As expected, there are many more peaks for a given energy range in the data from the TMO compared to Cu. This is a direct result of the complexity of the structure shown for both Cu and $Ca_{1.5}Sr_{0.5}RuO_4$ in Fig. 1(b).

The LEED *I-V* technique[3,4] is one of the most reliable experimental methods for surface structure determination. The strong interaction of low energy electrons, used as a probe in LEED, with atoms in the first few atomic layers of the surface (multiple scattering process) reduces the penetration depth of the electrons. This strong interaction makes LEED very surface sensitive but also makes it impossible to use any simple inversion of experimental data to determine the structure.[4] Therefore, surface structure determination by LEED is performed in an indirect way, by the comparison of intensity curves from diffracted spots as a function of incident electron energy [$I(V)$] with theoretically calculated curves for an assumed structure. This comparison is quantitatively evaluated by the use of a reliability factor or R factor,[4] with the one defined by Pendry (R_P) (Ref. 5) being the most commonly employed. If R_p=0 there is perfect correlation between the experimental and theoretical *I-V* curves. R_p=1 means that experiment and theory are uncorrelated. The lower the final R factor achieved, the more reliable is the structural determination. If $R_p \leq 0.3$, one can be confident in the structure (given a large enough experimental data set). The problem that motivated this paper is that for great part of LEED *I-V* studies of TMO surfaces the reported values of R_p are significantly larger (0.40–0.60).[6]

The multiple scattering theory currently used in LEED is based on the muffin-tin (MT) potential approximation[3,4] for individual atomic scattering potentials. In this approach, the potential inside a radial distance from the nucleus (MT radii) is spherically symmetrized and the potential in the interstitial region is assumed to be constant. A theoretical *I-V* curve is obtained by calculation of the electron scattering from individual atoms in the surface of the crystal, modeled by a spherical symmetric MT potential which yields the scattering phase shifts.[3,4] The determination of phase shifts for metallic systems follows a straightforward approach, where the MT sphere radius is defined as half of the shortest distance between the nearest neighbors. In the case of metallic alloys, the respective MT radii for the distinct atomic species are defined from the neutral atomic radii proportional to the lattice parameters of the alloy. The electronic densities employed in the MT potential calculations are those obtained for neutral atoms, usually from atomic self-consistent rela-

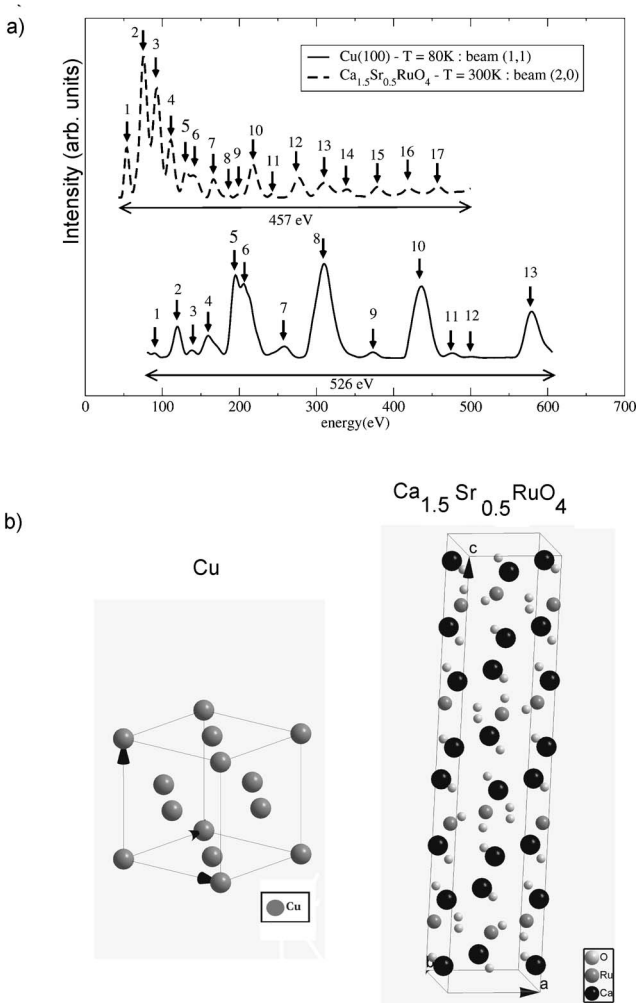

FIG. 1. (a) Typical $I(V)$ curves for Cu(100) and $Ca_{1.5}Sr_{0.5}RuO_4(001)$ systems. The $I(V)$ curve for the metal oxide surface presents a larger number of peaks (17, 13 for Cu), even with a shorter energy range (457 eV, 526 for Cu) due to the complexity of its structure. (b) Bulk unit cells for Cu and $Ca_{1.5}Sr_{0.5}RuO_4$.

tivistic calculations. However, in the calculation of phase shifts for metal oxides, effects of the charge transfer between oxygen and metal atoms must be taken into account. The charge transfer alters the effective radii of the ionic chemical species, i.e., the metallic cation will have a smaller radii than its neutral phase while the O^{-2} anion will have a larger radii than a neutral oxygen atom.

In the late 1970s, several papers addressed the issue of calculating phase shifts for metal oxides.[7–10] In these papers, the MT radii for metal cations and O^{-2} were arbitrarily adjusted in order to reach a good theory-experiment agreement. The use of electronic densities for neutral atoms and ions in the MT potential calculations were also investigated. In attempts to produce an ionic solution for the electronic charge densities, the occupancy of individual atomic states were altered. Only a small difference was observed in the final *I-V* curves generated with either neutral or ionic electronic densities. The choice of the MT radii seems to be more critical than the choice of atomic configuration.[7] However, all comparisons performed in these works were only qualitative, with the theory-experiment agreement evaluated visually as the use of reliability factors was not yet commonly employed.

A very recent paper presented a self-consistent approach for calculating the phase shifts for the $TiO_2(110)$ system.[11] An *ab initio* calculation was performed for bulk TiO_2 leading to ground state charge densities which are used as an initial guess for the MT radii (critical values) for both the Ti and O. The values obtained by this procedure do not correspond to either atomic or ionic radii. The MT radii obtained are used in an self-consistent Korringa-Kohn-Rostoker (KKR) calculation,[12] using the local density approximation (LDA) and leading to the self-consistent phase shifts. The resulting phase shifts are expected to take into account the charge transfer between the Ti and O ions in a more accurate way than simply assuming an ionic electronic distribution.

A third approach, which we will adapt in this paper, is where an optimized MT potential is proposed in which the spherical MT wells obtained by Mattheiss prescription include preassigned surface core level shifts and are continuously connected with a fiat interstitial potential.[13] Fundamental for the MT optimization is the condition that the local electron distribution of MT wells and interstice equilibrates the positive nuclear background charge. Critical to this procedure is the observation that the MT radii are energy dependent in order to generate a continuous potential at the MT radii and avoid undesired scattering resonance features in the phase shifts. The interstitial potential, related to the real part of inner potential (V_{0R}) as defined in LEED, is energy dependent due to the adoption of exchange-correlation approach (Hedin-Lundquist[14] or Sernelius[15]). We will show in this paper that this optimized MT potential approach is suitable for the application of LEED *I-V* to metal oxides. It overcomes several problems; defining a MT radii, and avoiding resonance effects due to discontinuities in the potential. It also allows in a natural way for the inclusion of an energy dependent real part of the inner potential.

II. EXPERIMENTAL PROCEDURES

The LEED *I-V* data were acquired in an ultra high vacuum chamber equipped with a computer controlled LEED diffractometer. A $Ca_{1.5}Sr_{0.5}RuO_4$ single-crystal sample (grown by the floating zone technique) was cleaved *in situ* under a base pressure of 2×10^{-10} Torr, producing a mirror-like (001) surface and generating sharp (1×1) LEED patterns as shown in Fig. 2. Details of the cleavage process have been described elsewhere.[16] In short, the sample was attached to a sample holder by the use of a silver epoxy with a metal post epoxied to the top of the crystal. The sample was cleaved by breaking off the attached post, producing a clean $Ca_{1.5}Sr_{0.5}RuO_4$ surface. After cleaving, the sample was introduced into a LEED chamber maintained with a base pressure of 5.0×10^{-11} Torr.

The sample position was adjusted, using the rotation and tilt angles available on the sample holder, in order to reach a normal incidence geometry for the primary electron beam. Exceptional alignment was reached as reflected by the fact that symmetrically equivalent beams agreed within a R_p of

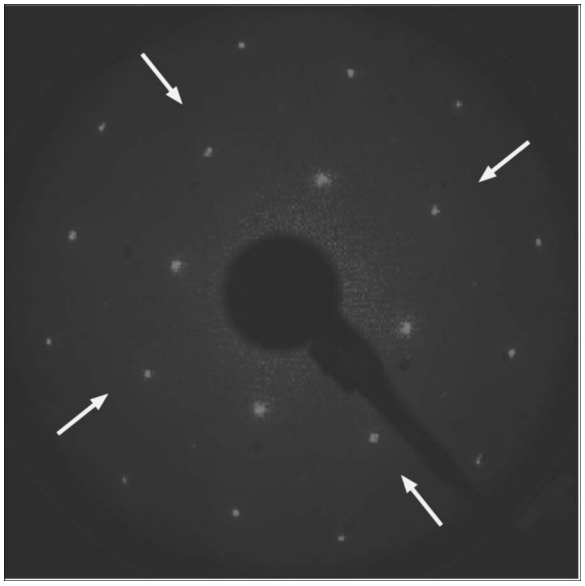

FIG. 2. LEED pattern for the $Ca_{1.5}Sr_{0.5}RuO_4(001)$ surface at a primary energy of 124 eV. The arrows indicate the directions of the two glide lines present in the diffraction pattern.

0.02. LEED patterns were collected at room temperature within an energy range 50–500 eV using a video-LEED system developed in-house.[17,18] The observed diffraction patterns have a *p*4*gm* symmetry, in contrast to the *p*2*gg* plane group symmetry that would have been anticipated from a bulk terminated (*I*41/*acd* tetragonal symmetry) $Ca_{1.5}Sr_{0.5}RuO_4(001)$ surface. Figure 3(a) shows the expected bulk termination and the *p*2*gg* plane group symmetry. The higher symmetry observed at the surfaces is due to the layered structure presenting two different terminations [Fig. 3(a)]. Figure 3(b) shows a large area scanning tunneling microscopy (STM) image, showing a step height corresponding exactly to the distance between the top of an octahedra layer to the top of the next one (6.2874 Å). These two terminations are related to each other by a simple 90° rotation, as can be seen in Fig. 3(a). Since the resulting LEED diffraction pattern is produced by both terminations, the symmetry is *p*4*gm*. Both LEED *I-V* and STM indicated that the terraces corresponding to both terminations were present in equal abundance. This assumption was further confirmed during the structural determination process where an equal weighted mixture of theoretical *I-V* curves from both terminations produced the best theory-experiment agreement. Here and in the analysis we assume an incoherent superposition of these two symmetries.

I-V curves were extracted from digitized diffraction patterns and subsequently smoothed using a five-point least-squares cubic polynomial algorithm and normalized to the electron gun current. Symmetrically equivalent beams, according to the resulting *p*4*gm* symmetry, were then averaged leading to a total energy range of 2687 eV using eight nonequivalent beams: (2,0), (4,0), (1,1), (2,2), (3,3), (1,3), (1,4), and (2,4).

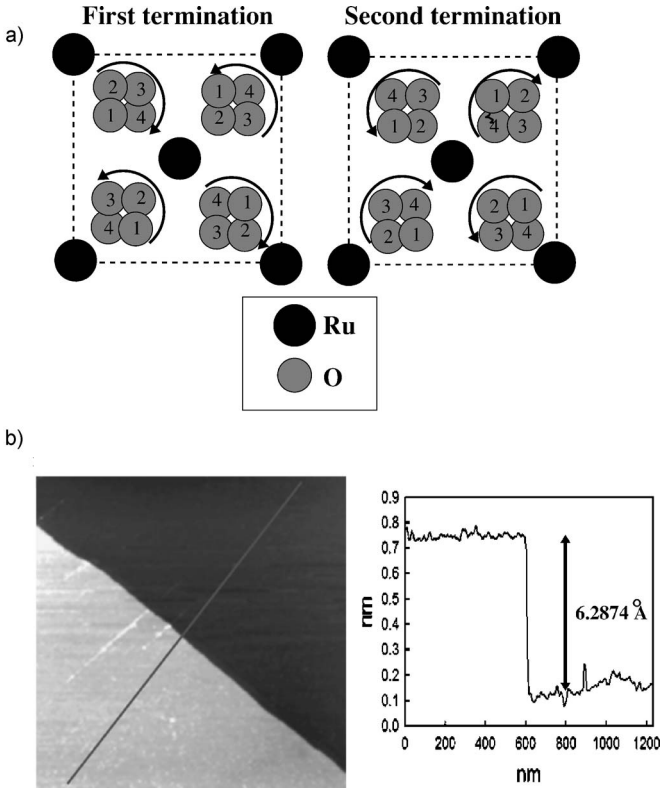

FIG. 3. (a) Two possible terminations for the $Ca_{1.5}Sr_{0.5}RuO_4(001)$ surface. Two *p*2*gg* symmetry terminations are related to each other by a 90° rotation and are generated by the relative stacking sequence of the rotated Ru-O layers. In this figure, just the Ru and O-plane atoms are represented for a best visualization. Labels 1, 2, 3, and 4 stand, respectively, for O atoms in the first, second, third, and fourth Ru-O planes [see Fig. 1(b)]. (b) STM image and height profile for the $Ca_{1.5}Sr_{0.5}RuO_4(001)$ surface. Large area terraces can be seen and are associated with the two existing terminations. The abrupt change in the height profile corresponds exactly to the distance from the top of one octahedra layer to the top of the other one (6.2874 Å) [see Fig. 1(b)].

III. THEORETICAL DETAILS, RESULTS, AND COMPARISON TO EXPERIMENT

The objective of this study is to develop a consistent procedure for calculating LEED *I-V* curves for TMO surfaces. The proposed procedure will be compared to other methods for calculation of phase shifts and tested by determining the structure of $Ca_{1.5}Sr_{0.5}RuO_4(001)$.

The approach of choice for calculating the phase shifts is the optimized MT potential method described in the previous section.[13] This will result in a consistent approach for calculating energy dependent MT radii. The MT radii presented in Fig. 4, were generated using this procedure. The local density approximation[14,15] was employed in the calculations and core level shifts were applied for varying radius and electron charge content (ionicity) of the MT wells. It is obvious from Fig. 4 that there is a dramatic difference in the MT radii for neutral vs Ru^{+4} and O^{-2}. Figure 5 shows the energy-dependent real part of the inner potential $V_{0R}(E)$ obtained from this procedure.

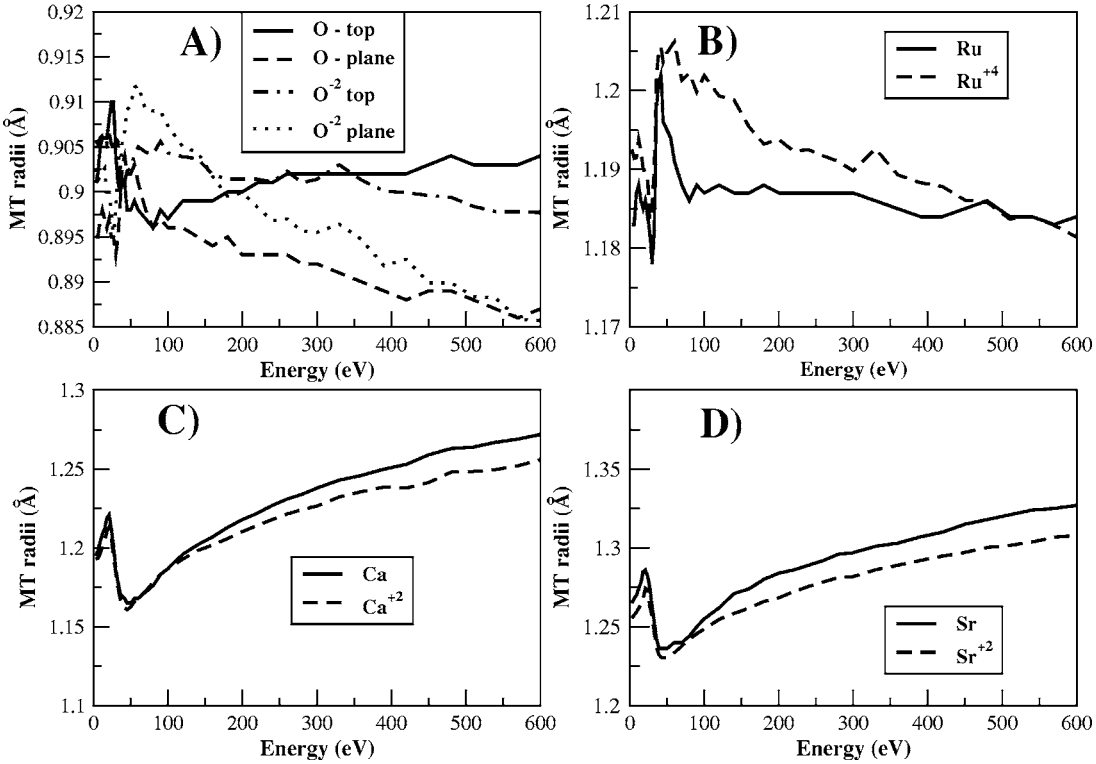

FIG. 4. MT radii values as a function of energy, as obtained in the optimized MT potential approach: (a) O and O^{-2} (top and plane), (b) Ru and Ru^{+4}, (c) Ca and Ca^{+2}, and (d) Sr and Sr^{+2}.

The second procedure for calculation phase shifts is to apply the commonly employed Mattheiss prescription,[19] but using two different methods for the definition of MT radii. The first method for MT radius determination consisted of running a DFT-GGA self-consistent calculation, using the PWSCF code[20] in order to obtain charge densities. The self-consistent calculation for bulk $Ca_{1.5}Sr_{0.5}RuO_4$ were performed using Vanderbilt ultra-soft pseudopotentials[21] with a cutoff energy of 25Ry on a $10\times10\times10$ points Monkhorst-Pack grid. The critical points in the charge densities obtained were used to define the MT radii for the Ca, Sr, Ru, and O ions. MT radii equal to 0.92, 1.07, 1.01, 1.31, and 1.40 Å were adopted for the Ru, O (octahedra top), O (Ru-O plane), Ca, and Sr species, respectively. These values do not correspond to either atomic or ionic radii, similar to the results obtained in the TiO_2(001) study.[11] Self-consistent relativistic calculations were then performed for Ca, Sr, Ru, and O atoms using neutral atom electronic distributions. The MT potential was then computed by the superposition of the atomic charge densities obtained in the previous step, assuming the MT radii previously obtained, and following Mattheiss prescription. The Barbieri/Van Hove phase shift package[22] was used for the calculations performed in this approach. In contrast to the TiO_2(110) study,[11] the first approach adopted in

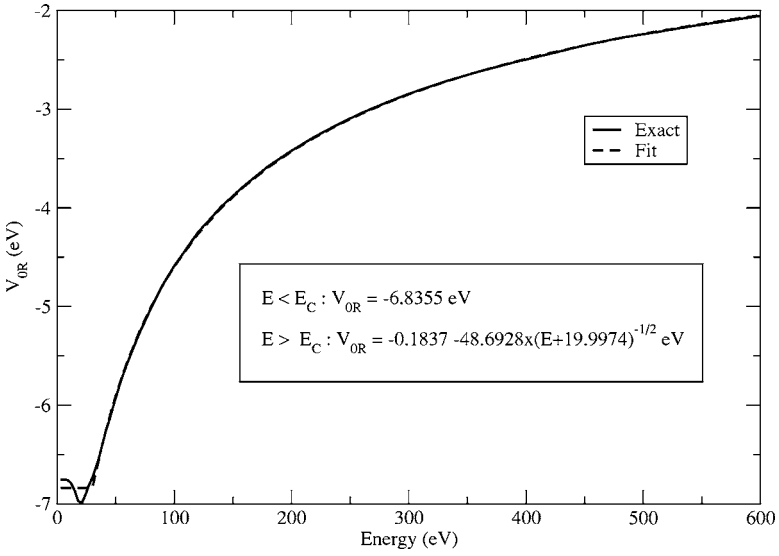

FIG. 5. Energy-dependent real part of inner potential obtained for $Ca_{1.5}Sr_{0.5}RuO_4$. The two curves correspond to the calculated (exact) and fitted ones, respectively. The functional form for the fitted curve, as suggested in Ref. 13, is presented in the graph.

this work used the *ab initio* self-consistent charge density calculations to simply define a more realistic MT radii for each ion. The second method employed for the MT radius definition, used effective empirical radii as defined by Shannon and Prewitt.[23] For comparison, the Barbieri/Van Hove code[22] was again used, adopting MT radii equal to 1.00, 1.16, 0.59, and 1.34 Å for the Ca, Sr, Ru, and O species respectively, as well as neutral atom electronic charge densities.

A standard LEED structural determination was performed where theoretical *I-V* calculations utilized the MT model for scattering potentials. The calculate *I-V* curves for a given structure were compared to the experimental data using the Pendry R_P factor as a measure of the goodness of the fit.

The $Ca_{1.5}Sr_{0.5}RuO_4(001)$ surface structure optimization was performed using a grid search in which the atoms of the first octahedra layer were vertically displaced (for a total of six structural parameters). The RuO_6 octahedra was also rotated along the Ru-top oxygen axis with all displacements maintaining the *p*2*gg* symmetry (resulting in *p*4*gm* with the two terminations). The grid search for the vertical displacements was performed in three steps: (1) exploring parameter space volume of ±0.06 Å per parameter; (2) a reiteration of parameter space volume of ±0.06 Å per parameter starting from the deepest R_P minimum found in the previous step; (3) a refined grid search in a reduced ±0.02 Å per parameter volume. At every one of the three steps a grid search for the rotation angle was performed for the optimum structure.

Debye temperatures were determined from the mean square atomic displacements obtained via neutron scattering experiments[24,25] with values of 325 K, 605 K, 355 K, and 237 K for the Ru, O, Ca, and Sr elements, respectively. An imaginary inner potential (V_{0I}) equal to −5.0 eV was also adopted in this first step of the calculations. In all investigated situations, even those with an energy-dependent real part of inner potential $[V_{0R}(E)]$, a constant contribution to the interstitial potential was optimized during the structural searches, starting from an initial value of −10.0 eV. The average T-matrix approximation (ATA)[26,27] was implemented to account for the Ca/Sr mixing presented by $Ca_{1.5}Sr_{0.5}RuO_4$ and all calculations have been performed using a total of ten phase shifts. The full dynamic LEED calculations were performed using the symmetrized automated tensor LEED code (SATLEED),[22] modified to include the energy dependence correction to the real part of the inner potential.[28]

A final refinement incorporating an energy dependent imaginary part of the inner potential $[V_{0I}(E)]$ was calculated in terms of the inelastic mean free path (λ_{IMFP})[29–34] according to

$$V_{0I} = \frac{1}{2\lambda_{IMFP}}\left[2(E - V_{0R}) + \frac{1}{4\lambda_{IMPF}^2}\right]^{1/2}, \qquad (1)$$

with E and V_{0R} being the kinetic energy and real part of the inner potential. The "module eimfp" code[35] was used for this calculation, using the National Institute of Standards and Technology (NIST) available data on Inelastic Mean Free Path (IMFP).[36] Since there is no mention of an energy dependent real inner potential $[V_{0R}(E)]$ in the NIST available data and taking into consideration the degree of approximation associated with the λ_{IMFP} calculation, it turns out that it is reasonable to assume a constant value for V_{0R}. An energy averaged value for the real part of the inner potential was obtained from the $V_{0R}(E)$ data previously discussed. The energy dependent imaginary part of the inner potential will be adopted as a refinement in the calculation of the theoretical $I(V)$ curves. Again the SATLEED code[28] was modified to include this correction. The $V_{0I}(E)$ and $V_{0R}(E)$ corrections will be important to obtain a reasonable R_P.

TABLE I. Final Pendry R factor values obtained using the different approaches adopted for phase shifts and V_{0R}. The values here presented are associated with the same final structure (Table II). In all situations, except 1(b), the imaginary part of the inner potential (V_{0I}) was assumed constant (−5.0 eV).

Situation	Final R_P
1(a): Optimized MT potential and $V_{0R}(E)$ Neutral atom electronic densities	0.31
1(b): Optimized MT potential with $V_{0R}(E)$ and $V_{0I}(E)$ Neutral atom electronic densities	**0.28**
1(c): Optimized MT potential and $V_{0R}(E)$ Ion electronic densities	0.31
1(d): Optimized MT potential and V_{0R} constant Neutral atom electronic densities	0.35
2(a): *Ab initio* MT radii and V_{0R} constant Neutral atom electronic densities	0.39
2(b): *Ab initio* MT radii and $V_{0R}(E)$ Neutral atom electronic densities	0.36
2(c): Empirical MT radii with V_{0R} constant Neutral atom electronic densities	0.43
2(d): Empirical MT radii with $V_{0R}(E)$ Neutral atom electronic densities	0.41

The second approach consisted in adopting the typical Mattheiss prescription with MT radii determined from two different methods. A total of eight distinct situations were investigated using different combinations of phase shifts and real and imaginary inner potentials. There are four situations explored using the optimized MT potential:[13] 1(a) phase shifts obtained from neutral atom electronic distributions and $V_{0R}(E)$; 1(b) phase shifts obtained from neutral atom electronic distributions, $V_{0R}(E)$ and $V_{0I}(E)$; 1(c) phase shifts obtained from ionic electronic distributions (Ru^{+4}, O^{-2}, Ca^{+2}, Sr^{+2}) and $V_{0R}(E)$; 1(d) phase shifts obtained from neutral atom electronic distributions and a constant value for V_{0R}; situation 1(d) was also explored to fully understand the role of $V_{0R}(E)$ in the final theory-experiment agreement. The final R_p values obtained for the best structure in all situations explored are presented in Table I. The structure will be described in the next section.

For the second approach (Mattheiss prescription), in the case where the MT radii were obtained from *ab initio* charge

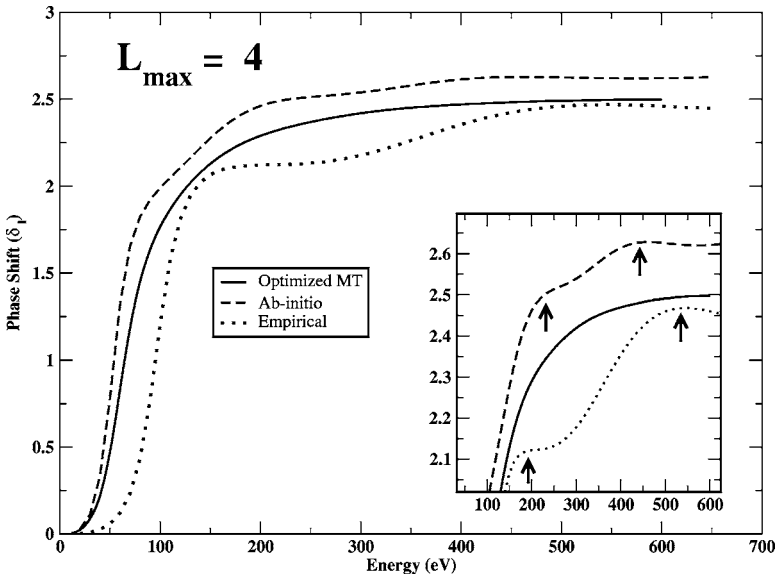

FIG. 6. Comparison between phase shifts obtained for the Ru element in $Ca_{1.5}Sr_{0.5}RuO_4$, for an *l* (angular momentum) value equal to 4. Only the optimized MT approach (Ref. 13) was able to produce smooth phase shifts. The phase shifts obtained with the Mattheiss prescription, employing both *ab initio* and empirical MT radii, presenting some undesirable resonance effects, as indicated in the graph by the arrows.

density calculations, two situations were explored: 2(a) phase shifts obtained from neutral atom electronic distributions and a constant V_{0R}; 2(b) phase shifts obtained from neutral atom electronic distributions incorporating $V_{0R}(E)$ obtained from the optimized MT calculations. For the case where MT radii were defined by empirical ionic radii,[23] the same two situations were again explored; 2(c) phase shifts obtained from neutral atom electronic distributions and a constant V_{0R}; 2(d) phase shifts obtained from neutral atom electronic distributions and use of the $V_{0R}(E)$ correction. Situations 2(b) and 2(d) were explored to investigate the importance of an energy dependent inner potential in the final theory-experiment agreement.

For all of the tests presented in Table I, the best theory-experiment agreement obtained was the one using the optimized MT potential approach with both $V_{0R}(E)$ (Ref. 13) and $V_{0I}(E)$ (Ref. 35) corrections included [situation 1(b)]. The lowest R_P achieved was 0.28. In order to understand this result it is important to remark that only the optimized MT potential approach[13] was able to lead to smooth phase shifts for all elements in $Ca_{1.5}Sr_{0.5}RuO_4$. A comparison between phase shifts obtained for Ru(l=4) with the optimized MT potential approach and with Matheiss prescription[19] (*ab initio* and empirical radii) is presented in Fig. 6. The phase shifts obtained with Matheiss' prescription display resonance features (see arrows), and are not smooth. These resonance effects arise from the fact that at the MT radii the crystal potential is not continuous, presenting steps, which accommodate quasistanding waves.[13] Within the optimized MT approach, the MT radii are optimized for every energy, in order to minimize the potential steps at the MT radii, leading to a common potential step at all MT radii and an energy dependent interstitial potential $V_{0R}(E)$. The MT potential of the structure is then made everywhere continuous by a common shift of all MT well potentials. Only insignificant resonance features remain due to the fact that the potential has a discontinuous first derivative at the MT radii. In the case of binary oxides, like in the Fe_3O_4 work by Barbieri *et al.*,[37] one can easily determine the MT radius values for the two atomic species in order to provide the continuity of the potential. However, in the case of systems like $Ca_{1.5}Sr_{0.5}RuO_4$,

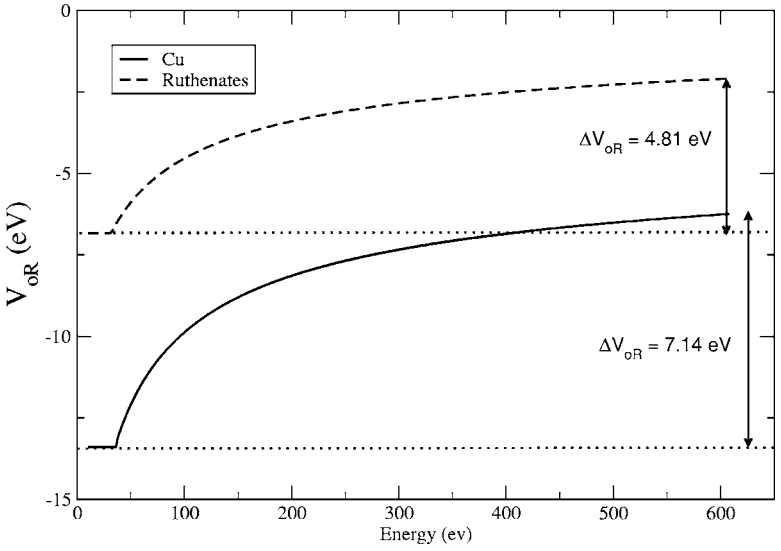

FIG. 7. Comparison between energy-dependent real part of inner potential $V_{0R}(E)$ for Cu and $Ca_{1.5}Sr_{0.5}RuO_4$. As it can be seen over the entire energy range, $V_{0R}(E)$ for Cu has a more significant change.

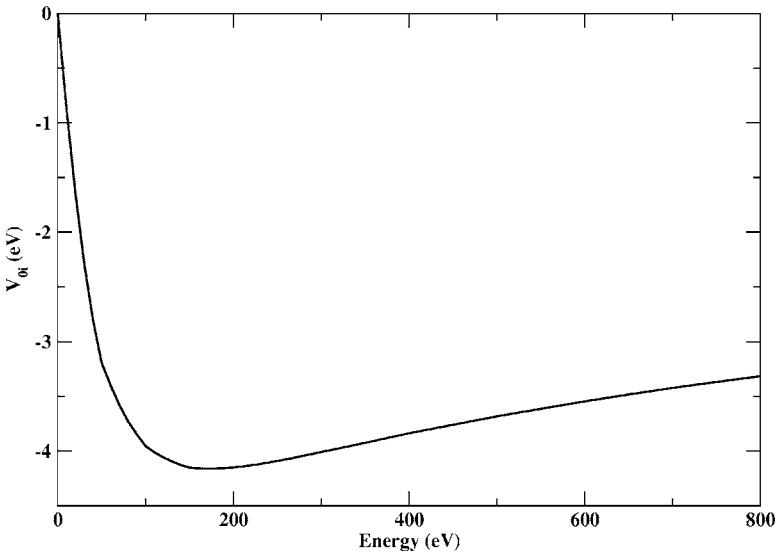

FIG. 8. Energy-dependent imaginary part of inner potential $[V_{0I}(E)]$ for $Ca_{1.5}Sr_{0.5}RuO_4$.

with a complex structure and a large number of distinct elements, a more systematic approach has to be adopted.

The use of ionic electronic distributions (Ca^{+2}, Sr^{+2}, Ru^{+4}, O^{-2}) presented in situation 1(c), in which the occupancy of atomic states were altered (versus states for neutral atoms) in the MT potential calculations, did not lead the structural search to a better R_p [same as in 1(a)], in agreement with Kinniburgh *et al.*[7] Employing *ab initio* self-consistent charge densities calculations to determine the MT radii [situation 2(a) with R_p=0.39] achieved a better final theory-experiment agreement compared to the empirical MT radii [situation 2(c) with R_p=0.43]. As in the TiO_2(110) work,[11] the charge densities critical points lead to radii that do not correspond to either atomic or ionic values. However, only the optimized MT potential approach [situations 1(a), 1(b), and 1(c)], in which MT radius values were optimized at every energy value, achieved an acceptable final theory-experiment agreement (R_P).

In order to distinguish the relative importance of the $V_{0R}(E)$ correction in the final theory-experimental agreement, a situation with a constant inner potential (V_{0R}) was explored using the same optimized MT radii phase shifts [situation 1(d)]. A final R_P of 0.35 was achieved, clearly indicating the importance of the energy dependence of the inner potential correction. Including the $V_{0R}(E)$ correction in the calculations performed with the *ab initio* and empirical MT radius phase shift approaches also reduced the value of R_P, from 0.39 to 0.36 for the *ab initio* case. The results obtained in this work indicate that the inclusion of the energy-dependent real inner potential correction is necessary to improve the theory-experiment agreement. The energy dependence of the inner potential played an important role in

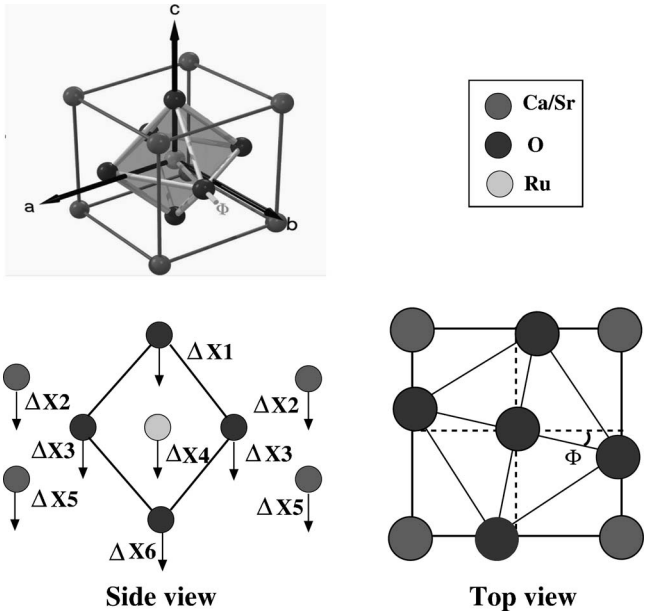

FIG. 9. Schematic presentation of the final structure obtained for the $Ca_{1.5}Sr_{0.5}RuO_4$(001) surface. The vertical atomic displacements as well as the rotation angle are presented.

TABLE II. Final structure for the $Ca_{1.5}Sr_{0.5}RuO_4$(001) surface as defined in Fig. 9. The final value for the Pendry R factor presented is for the situation where the approach of Ref. 13 was adopted for phase shifts with $V_{0R}(E)$ and $V_{0I}(E)$. The change in the Ru-O_6 octahedra volume, defined as the difference between bulk and surface values is also presented. The associated errors have been obtained according to Pendry.[5]

Parameter	Value
$\Delta X1$ (O top)	0.04±0.05 Å
$\Delta X2$ (Ca/Sr)	0.13±0.03 Å
$\Delta X3$ (O plane)	0.03±0.02 Å
$\Delta X4$ (Ru)	0.02±0.03 Å
$\Delta X5$ (Ca/Sr)	0.01±0.05 Å
$\Delta X6$ (O bottom)	0.00±0.06 Å
(rotation angle)	(12±5)°
	12.43° (bulk)
V (volume variation)	−0.10 Å^3
$V_{surf}-V_{bulk}$	(10.15–10.25) Å^3
R_P	(0.28±0.03)

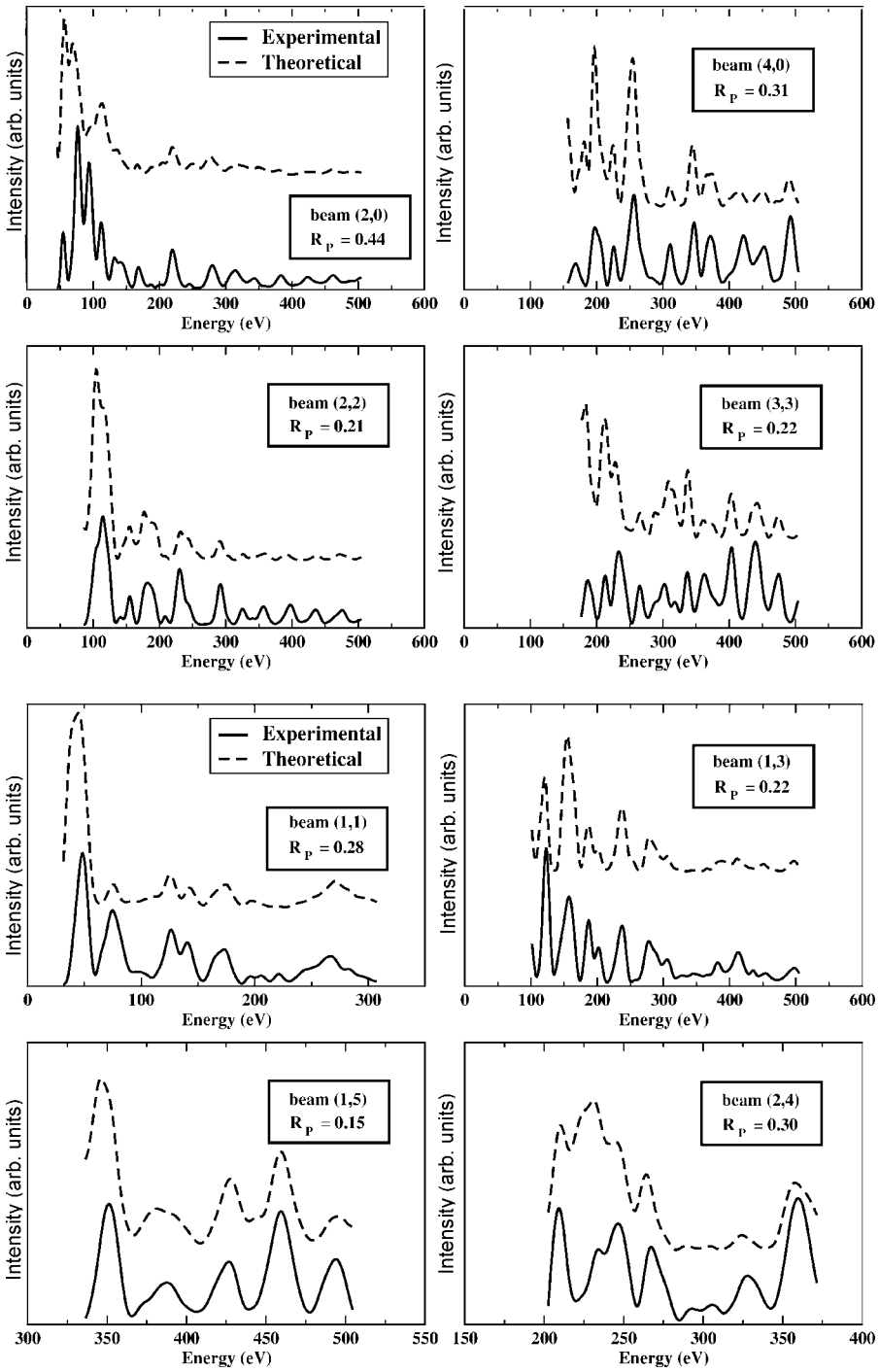

FIG. 10. Comparison between theoretical and experimental $I(V)$ curves for the best first structure.

the well-known case of the in-plane lattice parameter contraction for the Cu(100) surface.[38,39] In Ref. 38, a LEED structural optimization was performed, assuming V_{0R} as constant, and the results indicated a contraction of the surface in-plane lattice parameter. A later work,[39] employing V_{0R} constant and $V_{0R}(E)$ approaches, was able to determine that the in-plane lattice parameter contraction was an artificial effect from neglecting the energy dependence of the real part of the inner potential. It was also suggested that neglecting the $V_{0R}(E)$ correction could introduce errors in vertical (interlayer distances) and in-plane structural parameters.[39] However, in most LEED studies, V_{0R} is considered as an adjustable constant parameter with its energy dependence usually only considered in very fine structural searches ($R_P < 0.15$) with large energy ranges ($E > 300$ eV).[40]

It is important to understand why $V_{0R}(E)$ has such a prominent role in the final theory-experiment agreement for the $Ca_{1.5}Sr_{0.5}RuO_4(001)$ system since its value varies by only 4.81 eV within an energy range from 30 to 600 eV, as it can be seen in Fig. 7. If a comparison is made between the $V_{0R}(E)$ curves obtained for the Cu(100) (Ref. 13) and $Ca_{1.5}Sr_{0.5}RuO_4(001)$ systems, also shown in Fig. 7, one should expect the Cu(100) system to be more sensitive to an energy dependence of the inner potential since a more sig-

nificant change is observed (7.14 eV) for the same energy range. However, the inclusion of $V_{0R}(E)$ correction for the Cu(100) in the previous works[39] did not lead to a better theory-experiment agreement. One possible explanation for such a contradiction is as follows. From a comparison between typical experimental $I(V)$ curves for both systems, presented in Fig. 1(a), it is quite clear that the $Ca_{1.5}Sr_{0.5}RuO_4(001)$ surface $I(V)$ has a larger number of peaks. The $I(V)$ curve for Cu(100) presents 13 peaks within an energy interval of 526 eV while the one for $Ca_{1.5}Sr_{0.5}RuO_4(001)$ has 17 peaks within 457 eV. As the Pendry R factor is very sensitive to the peak positions,[5] neglecting the $V_{0R}(E)$ correction will introduce a systematic error in the theory-experiment comparison inducing higher R_p values. Although not observed in this work, neglecting the energy dependence of V_{0R} could even induce errors in the final structural parameter values, as suggested by Walter *et al.*[39] The larger number of peaks for $Ca_{1.5}Sr_{0.5}RuO_4(001)$ $I(V)$ curves can be explained, by the simple fact that the surface unit cell for this system contains a much more complex internal structure than that of Cu(100). In summary, in order to obtain higher accuracy in LEED surface structural determination for metal oxides, the energy dependence of the real part of inner potential must be taken into account. A high accuracy is required in the surface structure determination of systems like $Ca_{1.5}Sr_{0.5}RuO_4(001)$ since small variations in their structure can lead to dramatic changes in their physical properties.[24,25]

Another important point is that systems like $Ca_{1.5}Sr_{0.5}RuO_4$ present relatively high Debye temperatures[24,25] for the individual elements and consequently also present wide energy ranges for the individual $I(V)$ curves, even for data collected at room temperature. In such a situation, the use of the energy dependent real part of inner potential is especially important to achieve a good accuracy and to avoid systematic errors in the final structure.

The energy dependent imaginary part of the inner potential $[V_{0I}(E)]$ correction was included in the theoretical calculations for the $Ca_{1.5}Sr_{0.5}RuO_4(001)$ system as a final refinement. The $V_{0I}(E)$ for this system was calculated according to the procedure previously discussed and is presented in Fig. 8. With this refinement, the final theory-experiment agreement was improved, the final R_P value reduced from 0.31 to 0.28 [case 1(c) in Table I]. So, not only the real, but also the imaginary part of the energy dependent inner potential play a role in the final theory-experiment agreement. This result can be understood by considering the effect of the imaginary part of the inner potential in the damping of the diffracted intensities. Consider a diffraction peak in the 0–180 eV range on a background of a constant V_{0I} (peak centered at E_1) and on the background of $V_{0I}(E)$ (peak centered at E_2). Disregarding multiple scattering effects, one should expect $E_2 < E_1$, because in the case of the $V_{0I}(E)$ presented in Fig. 8, the left-hand side of the peak is less damped than the right-hand side. In other words, the peak rolls towards a lower absolute value for $V_{0I}(E)$, to a lower energy value. Analogously, a peak in the range 180–800 eV moves upward in energy towards a lower absolute value for $V_{0I}(E)$, to higher energy value. In this way peak positions at $E < 180$ eV and at $E > 180$ eV

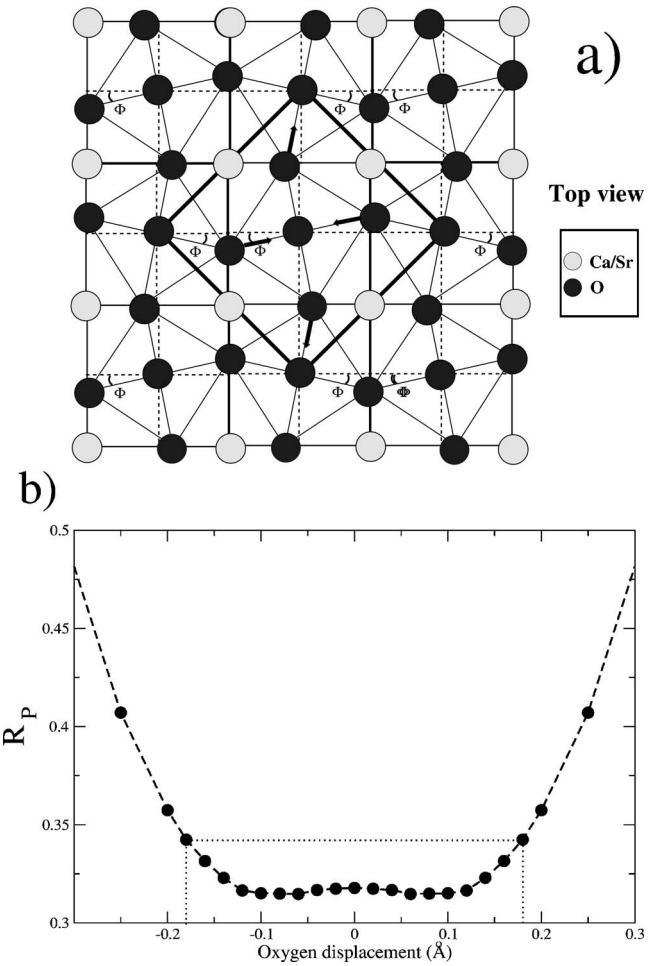

FIG. 11. (a) Distortion related to oxygen atom displacements along the Ru-O bonding, as allowed in the $p2gg$ plane symmetry. If the in-plane displacements for the four oxygen atoms are equal, the glide lines will not be excluded. (b) Pendry R factor as a function of the oxygen atom displacement. As it can be seen, there is no evidence for such distortion. The dashed lines indicate the associated error bar (±0.18 Å) for the oxygen displacement.

ranges move in opposite directions, to lower and higher energy values, respectively, giving a structural signal to Pendry's R factor.[5] This effect is obviously enhanced by the fact that the experimental $I(V)$ curves for $Ca_{1.5}Sr_{0.5}RuO_4(100)$ present a high number of peaks for energy range, as previously discussed.

All the results presented so far in this manuscript, regarding the optimized MT approach, have adopted phase shifts and $V_{0R}(E)$ obtained in a bulk calculation for the $Ca_{1.5}Sr_{0.5}RuO_4$ system. Slab calculations have also been performed, in which the MT radii of surface atoms were optimized in a different situation from the ones in the deeper layers, in order to try to mimic the break of the translational symmetry associated with the surface. However, no significant changes have been observed in either phase shifts and $V_{0R}(E)$.

IV. DISCUSSIONS AND CONCLUSIONS

All the structural searches performed utilizing the different approaches for phase shifts and V_{0R} lead (within associ-

ated errors) to the same final structure, displayed in Fig. 9 and tabulated in Table II. There is no reason to expect that this will in general be true for surfaces of TMOs. In this case the improvement in R_P resulted in a significantly smaller error on the determined distortions (compared to bulk). An acceptable final theory-experiment agreement was obtained for the case with optimized MT radii phase shifts with a $V_{0R}(E)$ and $V_{0I}(E)$ [situation 1(b)], with a best overall final R_P of 0.28. A comparison between theoretical and experimental $I(V)$ curves obtained for this approach is shown in Fig. 10.

From the data in Table II, it can be inferred that for the $Ca_{1.5}Sr_{0.5}RuO_4(001)$ no significant change in the Ru-O_6 octahedra shape has occurred at the surface. The surface octahedra rotation angle of $(12\pm5)°$ is the same as that in the bulk (12.43°).[24,25] However, the Ca/Sr ions in the surface display a large displacement inward (0.13 ± 0.03) Å, giving rise to a possible enhancement of a dipole moment or redistribution of charge related to the $(Ca/Sr)^{+2}$ and O^{-2} layers. Our studies[18] (to be published) on the $Ca_{2-x}Sr_xRuO_4$ series indicate that this distortion at the surface is a general property and can be related to a surface induced pressure.

The *p2gg* plane group symmetry at the surface allows for distortions in the Ru-O_2 octahedra planes with a lateral displacement of the oxygen in the direction of the Ru-O bond leading to two different Ru-O distances, as seen in Fig. 11(a). A grid search was performed in order to explore the existence of such a distortion in the octahedra. The results obtained, shown in Fig. 11(b), do not indicate the existence of any such Ru-O bond distortion.

Due to the layered structure of $Ca_{1.5}Sr_{0.5}RuO_4$ the (001) surface was expected to present a Ca/Sr-O layer termination after the cleavage process, as previously discussed. However, a Ru-O_2 plane terminated model, in which the top oxygens of the octahedra plus the Ca/Sr atoms are missing, was also investigated in this study. After structural parameters optimization, the Ru-O_2 plane terminated model resulted in a poor final theory-experiment agreement ($R_P=0.67$), yielding no evidence for such a termination. Possible changes in relative concentrations of Ca and Sr species in the first octahedra layer were also investigated and, within the sensitivity limitations of this study, no evidence was found for changes in relative concentrations.

In conclusion, we have developed a consistent procedure for evaluation of the scattering phase shifts for the LEED determination of the surface structure of TMOs and demonstrated it by determining the structure of the $Ca_{1.5}Sr_{0.5}RuO_4(001)$ surface. This study illustrated the importance of incorporating an energy dependent real and imaginary inner potential [$V_{0R}(E)$ and $V_{0I}(E)$].

ACKNOWLEDGMENTS

This work was supported by DOE, Division of Materials Sciences and Engineering (DMSE) through Oak Ridge National Laboratory (E.W.P., R.J., D.M., V.B.N.); DOE (DMSE) and NSF (DMR-0451163) (R.G.M.); and NSF (DMR-0346826) (J.Z. and L.C.).

*Electronic address: vnascime@utk.edu

[1] H. Yamada, Y. Ogawa, Y. Ishii, H. Sato, M. Kawasaki, H. Akoh, and Y. Tokura, Science **305**, 646 (2004).
[2] V. I. Ansimov, I. A. Nekrasov, D. E. Kondakov, T. M. Rice, and M. Sigrist, Eur. Phys. J. B **25**, 191 (2002).
[3] J. B. Pendry, *Low Energy Electron Diffraction* (Academic Press, New York, 1974).
[4] M. A. Van Hove, W. H. Weinberg, and C.-M. Chan, *Low-Energy Electron Diffraction Experiment, Theory and Surface Structure Determination* (Springer-Verlag, Berlin, 1986).
[5] J. B. Pendry, J. Phys. C **13**, 937 (1980).
[6] V. E. Henrich and P. A. Cox, *The Surface Science of Metal Oxides* (Cambridge, New York, 1994).
[7] G. G. Kinniburgh, J. Phys. C **8**, 2382 (1975).
[8] G. G. Kinniburgh and J. A. Walker, Surf. Sci. **63**, 274 (1977).
[9] M. Prutton, J. A. Walker, M. R. Welton-Cook, R. C. Felton, and J. A. Ramsey, Surf. Sci. **89**, 95 (1979).
[10] M. R. Welton-Cook and M. Prutton, J. Phys. C **13**, 3993 (1980).
[11] R. Lindsay, A. Wander, A. Ernst, B. Montanari, G. Thornton, and N. M. Harrison, Phys. Rev. Lett. **94**, 246102 (2005).
[12] A. Ernst, M. Lueders, W. M. Temmerman, Z. Szotek, and G. van der Laan, J. Phys.: Condens. Matter **12**, 5599 (2000).
[13] J. Rundgren, Phys. Rev. B **68**, 125405 (2003).
[14] L. Hedin and B. I. Lundqvist, J. Phys. C **4**, 2064 (1971).
[15] Kenneth W.-K. Shung, Bo E. Sernelius, and G. D. Mahan, Phys. Rev. B **36**, R4499 (1987).
[16] R. Matzdorf, Ismail, T. Kimura, Y. Tokura, and E. W. Plummer, Phys. Rev. B **65**, 085404 (2002).
[17] R. G. Moore and Z. Ward (private communication).
[18] R. G. Moore, Ph.D. thesis, University of Tennessee, 2006.
[19] L. F. Mattheiss, Phys. Rev. **133**, A1399 (1964).
[20] http://www.pwscf.org
[21] P. E. Blochl, Phys. Rev. B **41**, R5414 (1990); D. Vanderbilt, *ibid.* **41**, R7892 (1990).
[22] http://www.sitp.lbl.gov
[23] R. D. Shannon and C. T. Prewitt, Acta Crystallogr., Sect. B: Struct. Crystallogr. Cryst. Chem. **25**, 925 (1969).
[24] O. Friedt, M. Braden, G. André, P. Adelmann, S. Nakatsuji, and Y. Maeno, Phys. Rev. B **63**, 174432 (2001).
[25] O. Friedt, Ph.D. thesis, Université Paris XI, 2003.
[26] Y. Gauthier, R. Baudoing, M. Lundberg, and J. Rundgren, Phys. Rev. B **35**, 7867 (1987).
[27] S. Crampim and P. J. Rous, Surf. Sci. Lett. **244**, L137 (1991).
[28] V. B. Nascimento (private communication).
[29] C. J. Powell and A. Jablonski, J. Phys. Chem. Ref. Data **28**, 19 (1999).
[30] A. Jablonski and C. J. Powell, Surf. Sci. Rep. **47**, 33 (2002).
[31] S. Tanuma, C. J. Powell, and D. R. Penn, Surf. Interface Anal. **21**, 165 (1994).
[32] W. H. Gries, Surf. Interface Anal. **24**, 38 (1996).
[33] M. Seah and W. Dench, Surf. Interface Anal. **1**, 2 (1979).
[34] J. Rundgren, Phys. Rev. B **59**, 5106 (1999).

[35] J. Rundgren (private communication) (on request).
[36] C. P. Powell and A. Jablonski, NIST Electron Inelastic-Mean-Free-Path Database, National Institute of Standards and Technology, Gaithersburg, MD, 2000.
[37] A. Barbieri, W. Weiss, M. A. Van Hove, and G. A. Somorjai, Surf. Sci. **302**, 259 (1994).
[38] S. Muller, A. Kinne, M. Kottcke, R. Metzler, P. Bayer, L. Hammer, and K. Heinz, Phys. Rev. Lett. **75**, 2859 (1995).
[39] S. Walter, V. Blum, L. Hammer, S. Muller, K. Heinz, and M. Giesen, Surf. Sci. **458**, 155 (2000).
[40] LEEDFIT program manual, W. Moritz, M. Gierer, J. Landskron, T. Grnberg, M. Deschauer, Y. Gauthier, J. Rundgren, and H. Over (private communication).